# Spectral induced polarization of heterogeneous non-consolidated clays

A Mendieta, A Maineult, P Leroy, D Jougnot

# Spectral induced polarization of heterogeneous non-consolidated clays

**A. Mendieta[1], A. Maineult[1], P. Leroy[2], and D. Jougnot[1]**

[1]Sorbonne Université, CNRS, EPHE, UMR 7619 METIS, 75005 Paris, France
[2]BRGM, Department of Water, Environment, Processes and Analysis, 45100 Orléans, France

**Key Points:**

- Hydrogeophysics
- Electrical properties
- Numerical modelling
- Electrical anisotropy
- Electromagnetic theory

Corresponding author: Aida Mendieta, aida.mendieta_tenorio@sorbonne-universite.fr

**Abstract**

Clays are ubiquitously located in the Earth's near surface and have a high impact on the subsurface permeability. Most geo-electrical characterizations of clays do not take into account the heterogeneous nature of clay geological media. We want to better understand the influence of heterogeneities on the geo-electrical signature, thus we collected a dataset of spectral induced polarization (SIP) of artificial heterogeneous non-consolidated clay samples. The samples are made of illite and red montmorillonite in a parallel and perpendicular disposition (with respect to the applied electric field). Another sample is a homogeneous mixture composed of the same volumetric fraction of illite and red montmorillonite. For all the samples, the polarization is dominated by the red montmorillonite, given by the shape of the spectra (presence or lack of a peak at a particular frequency). We compared the experimental data with classical mixing laws and complex conductance network models to test how to better predict the SIP signature of such mixtures when the SIP spectra of the two components are known. The real conductivity is better predicted by the mixing laws, but the shape of the spectra (presence of polarization peaks at particular frequencies) is best predicted by the conductance network models. This study is a step forward towards a better characterization of heterogeneous clay systems using SIP.

## 1 Introduction

Clayey material exists in a variety of geologic formations and at various scales, from cap rocks to clay lenses or clay fractions in soils. Most laboratory geo-electrical characterizations of clays are done for a homogeneous mixture of clays, a mixture of sand and clays, or a clayrock sample from a particular geological formation (e.g., Cosenza et al., 2008; Ghorbani et al., 2009; Jougnot et al., 2010; Breede et al., 2012; Okay et al., 2014). However, most clay systems are heterogeneous and/or anisotropic (e.g., Wenk et al., 2008; Revil et al., 2013; Woodruff et al., 2014; Al-Hazaimay et al., 2016), thus these laboratory characterizations can fall short to predict the electrical signature of a heterogeneous and/or anisotropic clay system. There is a lack of geo-electrical laboratory experiments that better represent the complexity of clay systems. Additionally, there is a need to bridge the knowledge gaps between scales (clay sample to clay system). Moreover, there is a lack in our understanding of the electrical conduction and polarization phenomena at the mesoscopic scale, that is a scale larger than the typical pore size but smaller than the volume investigated by geophysical measurements (see Jougnot, 2020).

Physical properties of mixtures (hydraulic, electrical, elastic, among others) can be predicted with the use of mixing laws, such as Voigt (1910), Reuss (1929), and the self-consistent approach (Hashin, 1968). Mixing laws make use of a volumetric weighted average of the electrical properties of the individual components, without taking into account particular geometries. According to Knight & Endres (2005), simple approaches as these are able to properly predict the resulting electrical property from a sample with the electrical field in a parallel or perpendicular orientation with respect to its layering. Mixing models are a traditional, yet still effective approach used in geophysics (e.g., Berryman, 1995; Renard & de Marsily, 1997; Jougnot et al., 2018).

Another approach to bridge the scales in the geosciences is through pore network modeling (e.g., Bernabe, 1995; Day-Lewis et al., 2017; Jougnot et al., 2019). This approach when adapted to the electrical properties of media leads to impedance or conductance networks (e.g., Madden, 1976; Stebner et al., 2017). Maineult et al. (2018b), have related the pore properties (like pore radius) to electrical properties through phenomenological models, like a Pelton model (Pelton et al., 1978). In this study, we use the measured spectra for individual clays (see Mendieta et al., 2021) as input of each impedance of the network.

In Mendieta et al. (2021), five types of clays were studied at different salinities. Here, we use two of those types of clays, illite and red montmorillonite. In this work, we built synthetic samples in parallel (longitudinal disposition), series (transversal disposition), and homogeneous mixture configurations of both types of clays. We used complex conductance network modeling and mixing laws to predict the complex electrical conductivity response of the red montmorillonite and illite (initially at 0.01 M of NaCl) (see Mendieta et al., 2021). In this study, we consider extreme bounds of mixtures (Voigt and Reuss models) and heterogeneities, taking a step forward towards a better characterization of complex clay systems in situ.

To our knowledge, this use of mixing laws to describe the complex conductivity (real and imaginary parts) of clay mixtures from their pure components is novel. Indeed, traditionally, these formulas are used for the magnitude of the electrical conductivity only (e.g., Berryman, 1995). Similarly, the use of complex conductance networks to predict the electrical signature of laboratory measurements, particularly at this scale is novel.

## 2 Theory

### 2.1 Spectral Induced Polarization

SIP is a geophysical method that consists in injecting a sinusoidal-shaped electrical current into a rock sample and measuring the resulting electric potential difference and the phase-lag between the injected current and the potential difference, at different finite frequencies (mHz-kHz). The voltage-to-current ratio yields information about the electrical impedance of the rock sample, while the phase-lag ($\varphi$, in rad) informs about the capacity of the rock sample to reversibly store electrical charges (e.g., Revil, 2012). With the proper geometrical factor, we can obtain the electrical resistivity ($\rho$, in $\Omega$ m) or its inverse, the conductivity ($\sigma$, in S m$^{-1}$) of the sample. Generally, the complex electrical conductivity ($\sigma^*(\omega)$, or the complex resistivity $\rho^*(\omega)$) is frequency dependent and can be presented as:

$$\frac{1}{\rho^*(\omega)} = \sigma^*(\omega) = |\sigma|e^{i\varphi} = \sigma' + i\sigma'', \tag{1}$$

where $\omega$ is the angular frequency (rad s$^{-1}$), $i = \sqrt{-1}$ represents the imaginary unit, $|\sigma|$ is the amplitude of the measured signature (S m$^{-1}$), $\sigma'$ (S m$^{-1}$) is the real component of the electrical conductivity, and $\sigma''$ (S m$^{-1}$) is the imaginary component. The relation between $\omega$ and the frequency ($f$, Hz) is $\omega = 2\pi f$.

In the frequency range from the mHz to the kHz there is thought to be three polarization mechanisms (see Kemna et al., 2012; Loewer et al., 2017) giving rise to the measured polarization: the membrane polarization mechanism, the electrical double layer (EDL) mechanism, and the Maxwell-Wagner polarization mechanism. The membrane polarization mechanism happens at the lowest frequencies (mHz range) and arises from blockage of ions in pore throats (see Bücker & Hördt, 2013a,b). The EDL polarizes in the mid-frequency range (in the Hz range) due to the polarization of the Stern and diffuse layers around minerals surrounded by an electrolyte (see Leroy et al., 2017; Bücker et al., 2019). Finally, at the highest frequencies (kHz range) the Maxwell-Wagner polarization mechanism takes place at the interfaces of different phases in direct contact with each other (see Loewer et al., 2017).

### 2.2 Mixing laws

There are multiple ways to calculate the electrical signature of heterogeneous or homogeneous mixtures. Commonly used mixing laws in geophysics (for electric, elastic, magnetic, among many other physical properties) are the Voigt (1910), Reuss (1929), and self-consistent approach (Hashin, 1968) to mixtures (see Renard & de Marsily, 1997, for a review on permeability), the volume averaging approach (Pride, 1994; Revil et al., 2007), and the differential effective medium theory (e.g., de Lima & Sharma, 1992; Cosenza et al., 2008). With the differential medium theory, the effect of inclusions with their own electrical properties is added to a background with different electrical properties. The geometry of the whole mixture is modified by adding the inclusions iteratively, until a geometrical requirement is met, thus calculating the electrical property of the whole mixture. For the volume-averaging approach, the governing and constitutive equations of interest (e.g. Maxwell laws for electrical properties) are averaged in a representative elementary volume. Mixing laws are a simple, yet effective approach to calculate the resulting electrical properties from a volumetric weighted average of the individual components. We decided to use mixing laws due to their simplicity, yet effectiveness.

Here, we focus on the Voigt, Reuss, and self-consistent theory. For a mixture made of two materials, the resulting electrical signature will be bound (minimum and maximum) by the electrical signature of the individual materials. When the mixture is disposed in parallel (i.e., considering an analogous electrical circuit), we can use the Voigt (1910) approach to calculate the resulting electrical signature, that is:

$$\sigma_V^* = c\sigma_1^* + (1-c)\sigma_2^*, \tag{2}$$

where, $\sigma_V^*$ represents the complex electrical conductivity of the mixture disposed parallel to the applied electrical field, $\sigma_1^*$ represents the complex electrical conductivity of the first material, and $\sigma_2^*$ of the second material, and $c$ is the volumetric proportion of material 1 with respect of the whole volume of the mixture. For a series disposition (perpendicular to the applied electrical field), we use the Reuss (1929) approach, that is:

$$\sigma_R^* = \left(\frac{c}{\sigma_1^*} + \frac{1-c}{\sigma_2^*}\right)^{-1}, \tag{3}$$

where $\sigma_R^*$ is the complex electrical conductivity of the mixture disposed in series. Finally, when there is a homogeneous mixture of two materials, we can use the self-consistent (Hashin, 1968) approach, that is:

$$\sigma_{SC}^* = \sigma_2^* + \frac{3c\sigma_2^*}{3\sigma_2^* + (1-c)(\sigma_1^* - \sigma_2^*)}(\sigma_1^* - \sigma_2^*) \tag{4}$$

where $\sigma_{SC}^*$ is the complex electrical conductivity of the homogeneous mixture of two materials. In our case $c = 0.5$ for all mixtures, that is for equations 2, 3, and 4. Note that when $c = 0.5$, equation 2 becomes a simple arithmetic mean, and equation 3 becomes a harmonic mean. These expressions have previously been used for the amplitude of the electrical conductivity (e.g., Berryman, 1995), not for the entire complex conductivity (that is the real and imaginary part) in SIP laboratory measurements. It is worth mentioning that Kenkel et al. (2012) created a forward model for anisotropic media using mixing laws with complex conductivity to better understand field measurements of anisotropic media.

### 2.3 Complex conductance network modeling

To simulate the SIP signature of the clay mixtures, we additionally used complex conductance networks (see for instance Maineult et al., 2017; Maineult, 2018a; Maineult et al., 2018b, 2021). We designed a network on a regular 2D mesh (see the example given in Fig. 1). Each link of the network consists of a given complex conductance. By applying Kirchhoff's law (1845), we obtain a linear equation expressing the current continuity at each node of the network. Replacing the current in a given link by the product of the complex conductance of this link and the electrical potential difference between the two nodes delimiting this link, and applying the boundary conditions (i.e., the potential is equal to $V_0 e^{i\omega t}$, with $V_0 = 1V$ at the bottom and 0 at top, with no flux on the lateral faces, see Fig. 1), we can obtain a linear system that is solved for each angular frequency $\omega$ in order to get the potentials at the nodes. For more detail see Maineult et al., 2017, section 2.2. We impose a potential value at the top and bottom boundaries and deduce a flux. It is then straightforward to deduce the ratio of the potential difference applied between the two end faces to the computed total inflowing/outflowing current, as well as the phase-shift between these two quantities (please note that the full derivation for a square mesh can be found in Maineult et al., 2017, corrected by Maineult, 2018a). In the case of an illite and red montmorillonite mixture, we use the impedance spectra reported in Mendieta et al. (2021) for illite and red montmorillonite at 0.01 M NaCl (presented in Fig. 3). Please note that this type of modeling can be done for different types of connectivity (e.g., triangular, rectangular, or hexagonal mesh).

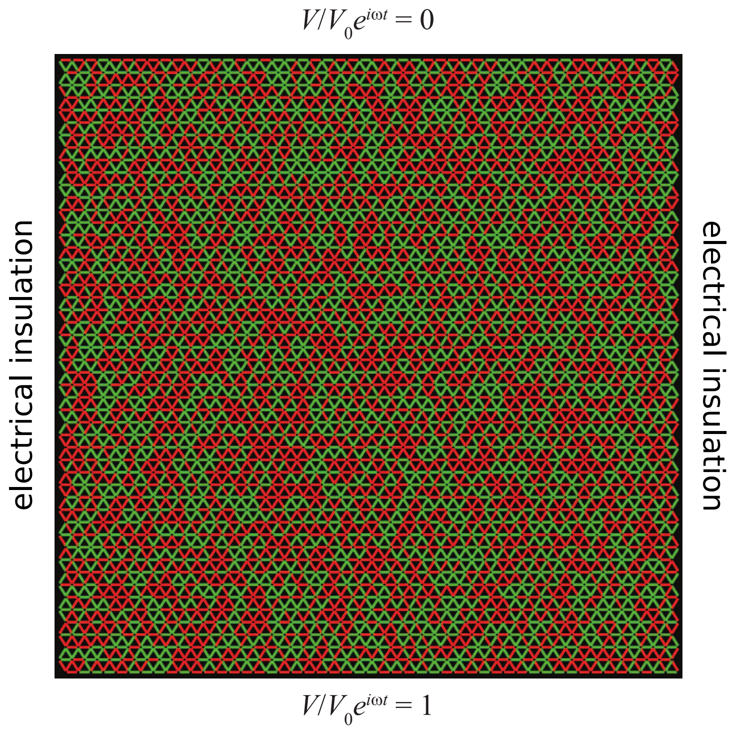


**Figure 1.** 50x50 triangular complex conductance network simulating a random homogeneous mixture of illite and red montmorillonite. The green links correspond to illite, the red ones to red montmorillonite.

## 3 Materials and Methods

### 3.1 Materials

The SIP responses of four (red and green montmorillonite, illite and kaolinite) types of clays have been characterized individually at different salinities in Mendieta et al. (2021). Based on their results, we used two clay types with a completely different behaviour (with respect to their electrical signature): illite and red montmorillonite. We also decided to use an initial salinity that would show a significant difference between both clay types.

An excessively high salinity would have created extremely conductive clay samples, yielding SIP data with high noise, and an excessively low salinity sample would have created important non-equilibrium in the pore-water chemistry (possible ion release from the interlayer space of clay tactoids as discussed in Mendieta et al., 2021). Thus we decided to use an initial salinity of $10^{-2}$ M of NaCl. As described in Mendieta et al. (2021), the clay samples follow an evaporation period, thus the salinity of the SIP measured clay sample is in the same order of magnitude as the initial salinity but not exactly the same.

A detailed description and analysis of the clays used in this study, with a detailed explanation of the laboratory protocol is presented in Mendieta et al. (2021). We will however, briefly describe the used materials and laboratory protocol.

In the present study we used two types of non-pure clays, a red montmorillonite and an illite. A chemical analysis of the clay samples shows that the red montmorillonite sample is made of: 66% smectite, 11% quartz, 18% microcline, 3% albite, and 1% magnetite. The illite sample is made of: 67% illite, 10% kaolinite, 10% microcline, and 12% calcite. The measured cationic exchange capacity (CEC) values are 135 meq/100 g for the red montmorillonite sample, and 47 meq/100 g for the illite sample. Finally, the measured specific surface area through the Brunauer-Emmett-Teller (BET) method is 71.09 $m^2/g$ for the red montmorillonite sample, and 101.60 $m^2/g$ for the illite sample. It is worth noting that the use of the BET method has proven to not be optimal for smectites, as the BET method is unable to probe the interlayer space. Specific surface area values proposed in the literature for smectites are in the range of 390-780 $m^2/g$ (see Tournassat et al., 2013).

### 3.2 Laboratory protocol

In this study we prepared three heterogeneous mixtures, and one homogeneous mixture of red montmorillonite and illite. For the heterogeneous mixtures, we located the individual clay types in two different arrangements: a transversal (Fig. 2b, or series arrangement) and longitudinal arrangements (Figs 2c and d, or parallel arrangements). We aimed at creating a 50-50% volume ratio, for each type of clay. For the creation of the heterogeneous mixtures, we created individual clay samples of illite and red montmorillonite, following the protocol proposed by Mendieta et al. (2021) (see their subsection 3.2). For the homogeneous mixture (Fig. 2a), there are extra previous steps in the laboratory protocol. This laboratory protocol consists in: a combination of clay powder and the aqueous solution, a period of at least 24 h for saturation and equilibrium of the mixture, mixing of the sample with an electric drill, disposition of the clay sample on top of a polyurethane foam until the correct water content is achieved through evaporation, the placement of the clay sample inside the sample holder for the SIP measurements, and finally the drying of the clay sample. For the homogeneous mixture, the extra previous steps are: mixing the dry clay powders of illite and montmorillonite with an electrical drill. Using the same mass proportions as in the 50-50% volumetric heterogeneous mixtures.

For the SIP measurements, all clay samples are placed in a cylindrical sample holder, the injecting electrodes are located on the sides of the cylinder, and the measuring electrodes are located on top of the cylinder casing (Fig. 2e). This is why we measured the SIP signature of two longitudinal heterogeneous mixtures, once the upper half (in contact with the measuring electrodes) was filled with illite (Fig. 2c), and once with red montmorillonite (Fig. 2d).

### 3.3 SIP measurement

We used the SIP-FUCHS III equipment (Radic Research, www.radic-research.de) for the SIP measurements. See Fig. 2(e) for a sketch of the SIP measuring setup. We utilized Cu-$CuSO_4$ non-polarizable electrodes as electric potential measuring electrodes. Indeed, in order to build the non-polarizable electrodes, we followed the procedure presented in Kremer et al. (2016), that is we filled a plastic tube with a gelified $CuSO_4$ solution. The dimensions of the electrodes are 5 mm diameter and around 10 cm in height. The bottom of the electrodes is plugged by a ceramic porous filter, and on the top by a rubber plug with an inserted copper wire. For the injecting electrodes we used two stainless steel cylinders that also served as covers of the sample holder. We made use of a four-electrode system for the SIP measurements, as according to Kemna et al. (2012) using a two-electrode system introduces unacceptably large errors in the measurement in our frequency range of interest. As presented in Fig. 2(e) the length of the sample holder is of 229.32 mm with a diameter of 43.20 mm. The electrodes are equally separated; we chose this configuration based on the recommendations presented in Zimmermann et al. (2008). We measured the SIP signature from 1 mHz to 20 kHz twice, separated by around

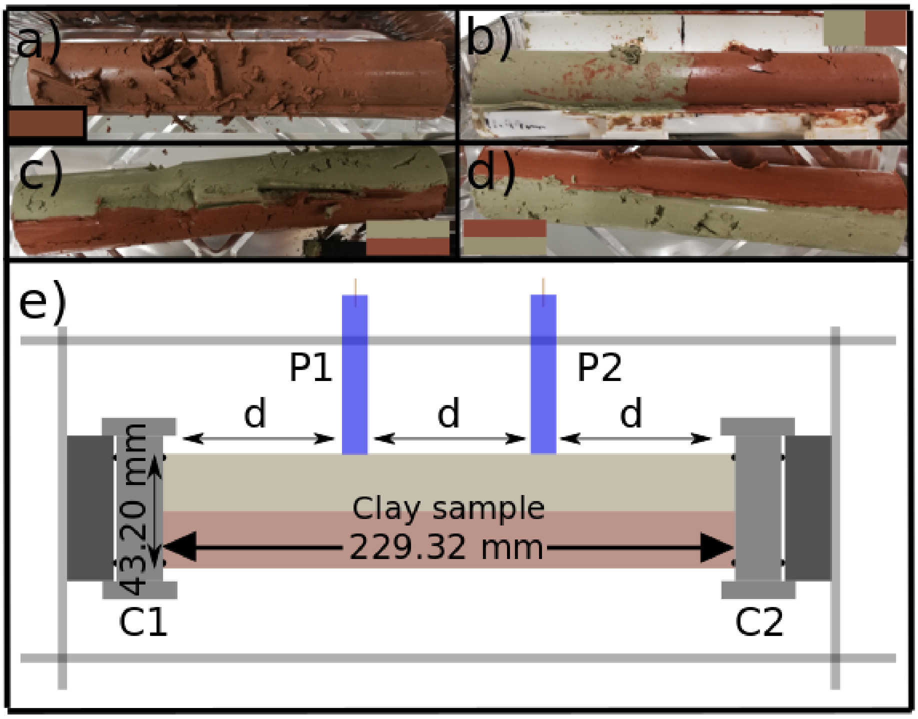


**Figure 2.** Different clay samples prepared in the laboratory. a) A homogeneous mixture of illite and red montmorillonite, b) heterogeneous-transversal mixture of illite and red montmorillonite, c) longitudinal mixture with illite on the side of the measuring electrodes, and d) longitudinal mixture with red montmorillonite on the side of the measuring electrodes. Note that these pictures correspond to the clay samples after taking them out of the sample holder. e) Sketch of the clay sample holder and external structure (grey lines), where C1 and C2 are the injecting electrodes, P1 and P2 are the potential electrodes. Note that this is merely a sketch of the SIP measurement setup and is not at a 1:1 scale.

24h. The SIP data we present in this work correspond to the second measurement, as the system is mostly equilibrated and the signature is then more stable.

### 3.4 Complex conductance network models

The principles of the complex conductance network models are explained in section 2.3. Fig. 1 represents a homogeneous mix of illite and red montmorillonite with a triangular mesh. Additionally, we modeled a complex conductance network where the top half was solely illite and the bottom solely red montmorillonite. We also modeled a complex conductance network with the right half corresponding to illite, and the left half corresponding to red montmorillonite. It is worth mentioning that the order of the location (which clay is located in which half) is irrelevant, as in this model there are no point measurements for the electric potential (opposite to laboratory measurements). For instance, locating the illite on the top or bottom will not alter the results, as the conductance network will yield the resulting electric potential difference of the system as a whole. Note that we performed the calculations for a triangular mesh (as shown in Fig. 1), but also for a rectangular and hexagonal mesh. The results of the rectangular and hexagonal meshes are presented in the supplementary information file. Overall, the triangular mesh proves to be the best option because it has the highest connectivity among the rectangular, hexagonal, and triangular meshes. The triangular mesh (highest connectivity) presents the best fit between data and models, this can be interpreted as our sample (non-consolidated clays) having high connectivity themselves (see supplementary information, Fig. S3). Additionally, the meshes used in this contribution had a $50 \times 50$ size. Please note that after some tests it appears that the mesh size of $50 \times 50$ is sufficient to converge to a unique response. For additional information, see Maineult et al. (2017), and supplementary information (Fig. S4).

## 4 Results

### 4.1 Complex conductivity measurements

The results of the SIP measurements of the homogeneous and heterogeneous mixtures are presented in Fig. 3. Note that the datasets of the individual clay types, illite and red montmorillonite, have been added for reference, these data were taken from Mendieta et al. (2021). From the results we can see that all mixtures of illite and red montmorillonite fall in between the data points of illite and red montmorillonite, which is expected. Here, we measured the SIP signature of a homogeneous mixture of illite and red montmorillonite, and three heterogeneous mixtures placed in a longitudinal (parallel) and transversal (series) manner. For the longitudinal set-ups, we conducted two measurements, one locating the illite on the top portion of the sample holder (near the measuring electrodes, see Fig. 2c) and the second with the red montmorillonite on top (see Fig. 2d). We can see that these longitudinal measurements do not match perfectly, and that makes sense; we do not have the same sensitivity immediately at 1 or 2 cm below the measuring electrodes. However, we see that the longitudinal mixture with the illite on the top portion of the sample holder, is not identical to the measurement of solely illite, that means that the longitudinal mixture with the illite on top is still affected by the red montmorillonite below. If we take a look at Fig. 3, we verify that the transversal mixture is in fact closer in both value and shape to the individual illite than the longitudinal mixture with illite on the top. By shape, we refer to the presence or lack thereof a peak in the phase or imaginary conductivity near 10 Hz. This also proves that the red montmorillonite in the longitudinal mixture with illite on the top affects the SIP signature (i.e. the SIP measurement is sensitive to the red montmorillonite on the bottom of the sample holder).

The bounds of the electrical in-phase conductivities of the mixtures are the electrical conductivities of both illite and red montmorillonite (see Fig. 3). The electrical conductivities at 1.46 Hz of the red montmorillonite and illite are 0.39 S $m^{-1}$ and 0.16 S $m^{-1}$, respectively. The corresponding electrical conductivity values of the mixtures at 1.46 Hz are: 0.22 S $m^{-1}$ (transversal arrangement), 0.24 S $m^{-1}$ (longitudinal arrangement with the illite on the top portion of the sample holder), 0.28 S $m^{-1}$ (longitudinal arrangement with the red montmorillonite on the top portion of the sample holder), and 0.26 S $m^{-1}$ (for the homogeneous arrangement). We verify that all mixtures fall between the bounds. For the phase, in the lower frequencies (1 mHz to 5.9 Hz) all the spectra resemble. However in the higher frequencies (above 5.9 Hz), we can see a clear difference between the spectra of each mixture. At 750 Hz, the phase of the illite sample is of 4.7 mrad, and of the red montmorillonite is 14.8 mrad. The transversal dataset (black dots) is the one that is closer to the value of the phase of the illite and it is 10.8 mrad. The rest of the mixtures are quite closer in value to the red montmorillonite.

Note that the mixtures and the individual complex conductivity spectra of illite and red montmorillonite were collected at different temperatures. The illite SIP data were collected at a temperature of around 21.9 °C, and the montmorillonite SIP data were collected at around 23.1 °C. The heterogeneity SIP dataset was collected at around 18.9 °C. We corrected the heterogeneity dataset to a 22.5 °C temperature. We used the temperature correction proposed by Hayley et al. (2007). The maximum percentage change between the measured and the temperature corrected conductivity for all datasets is of 8.8%. It is worth mentioning that we only corrected the conductivity magnitude, because to the best of our knowledge there is not a temperature correcting procedure for the phase. Although it has been pointed out that temperature influences the complex conductivity of a geo-material (e.g., Zisser et al., 2010; Bairlein et al., 2016; Iravani et al., 2020), there is still a need to find a petrophysical law or relation to correct for it (see Kemna et al., 2012).

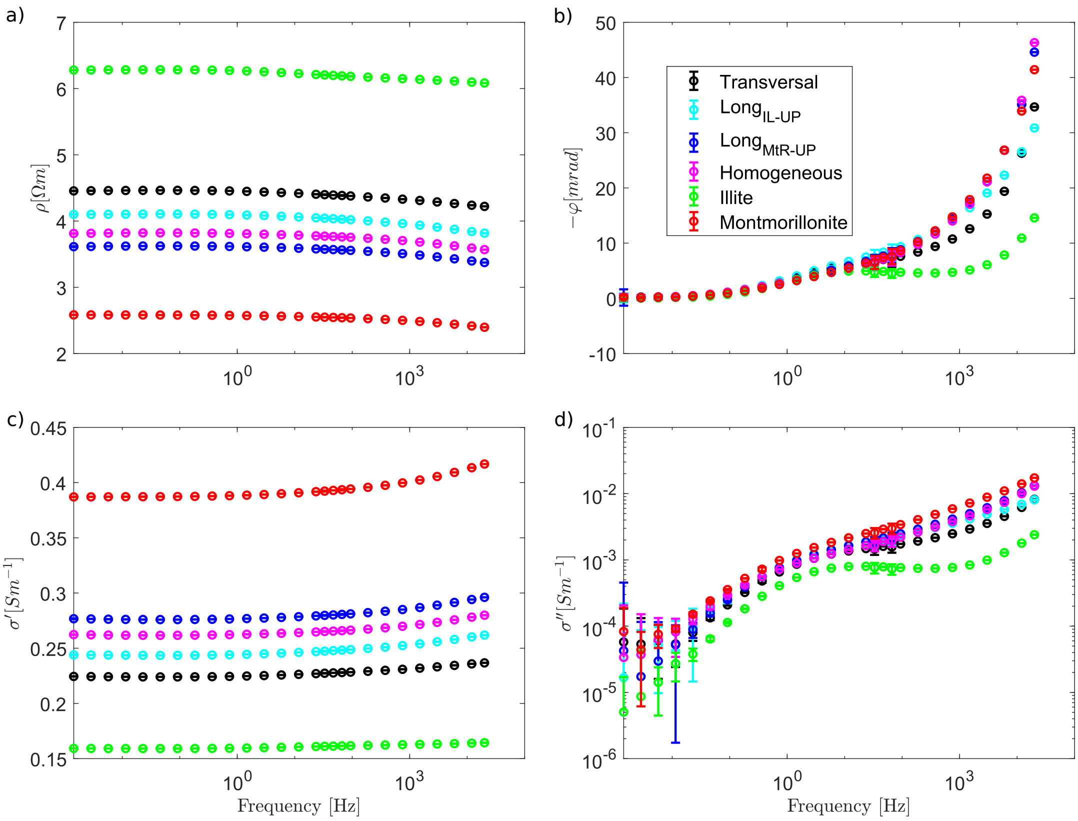


**Figure 3.** SIP data, as a) amplitude, b) phase, c) real component and d) imaginary components of the complex conductivity. The illite and red montmorillonite clay samples have been taken from Mendieta et al. (2021). The rest of the datasets here presented are a homogeneous mixture of illite and red montmorillonite, as well as three heterogeneous mixtures: a transversal mixture (series), and two longitudinal mixtures (parallel), one with illite in contact with the measuring electrodes (Long$_{\text{IL-UP}}$), and one with red montmorillonite (Long$_{\text{MtR-UP}}$).

## 4.2 Complex conductance network modeling results

As mentioned in section 3.4, we modeled the complex conductivity of three different mixtures: a homogeneous mixture, a transversal-heterogeneous mixture, and a longitudinal-heterogeneous mixture. Note that for the complex conductance network models we cannot obtain a model for illite or red montmorillonite on the side of the measuring electrodes, because for complex conductance network models, there is no point measure. In the mesh, the side on which each clay is located does not affect the end result of the model. For each type of mixture we considered three types of mesh for the numerical modeling (with a different connectivity each): a rectangular, a hexagonal, and a triangular mesh. In this contribution we will only present the simulations results using the triangular mesh, the simulations using other meshes are presented in the supplementary material. In Fig. 4 we present the SIP data overlaid by the results of the complex conductance network models; that is the real and imaginary part of the conductivity (Figs 4a and b, respectively), and the normalized real and imaginary conductivities (Figs 4c and d, respectively). We have normalized the spectra by the conductivity value at 1.46 Hz. We chose the closest value to 1 Hz, as this is a widely used value in geophysics (e.g., Zanetti et al., 2011).

Both model and data (Fig. 4) resemble more the red montmorillonite than the illite complex conductivity spectra, in shape (i.e. lack of a peak in the phase and imaginary conductivity near 10 Hz). It appears that the red montmorillonite affects more the resulting polarization than the illite in a mixture with equal proportions, whether it is a homogeneous mixture or a heterogeneous one. We also notice that the fit is not perfect between the prediction of the triangular conductance network model and the data; it is possible that the difference is due to 3D effects while the conductance network is in 2D. However, for the whole spectra the difference between model and data, for the real conductivity remains below 0.01 S $m^{-1}$. Al-Hazaimay et al. (2016) measure the SIP signature of two anisotropic systems and perform a numerical model. They add a correction factor to be able to compare 2D anisotropic models to real anisotropic systems measured in the laboratory. Due to our measuring setup, we are unable to apply such correction.

### 4.3 Comparison with mixing laws

We additionally modeled the SIP signature of the different mixtures using the mixing laws proposed by Voigt (1910), Reuss (1929) and Hashin (1968). In Fig. 5, we confront the SIP data versus these models. Note that we present a $\text{Voigt}_{IL-UP}$ and a $\text{Voigt}_{MtR-UP}$ model. We use bulkhead connectors in order to fix the measuring electrodes in the sample holder during the SIP measurement. For this reason on the half-cylinder side next to the electrodes a small volume corresponding to the nut of the bulkhead connector must be subtracted, that is both halves do not have equal volume. The volume used by the bulkhead connector is 0.184 $cm^3$. For the case of both volume fractions being equal $c =$

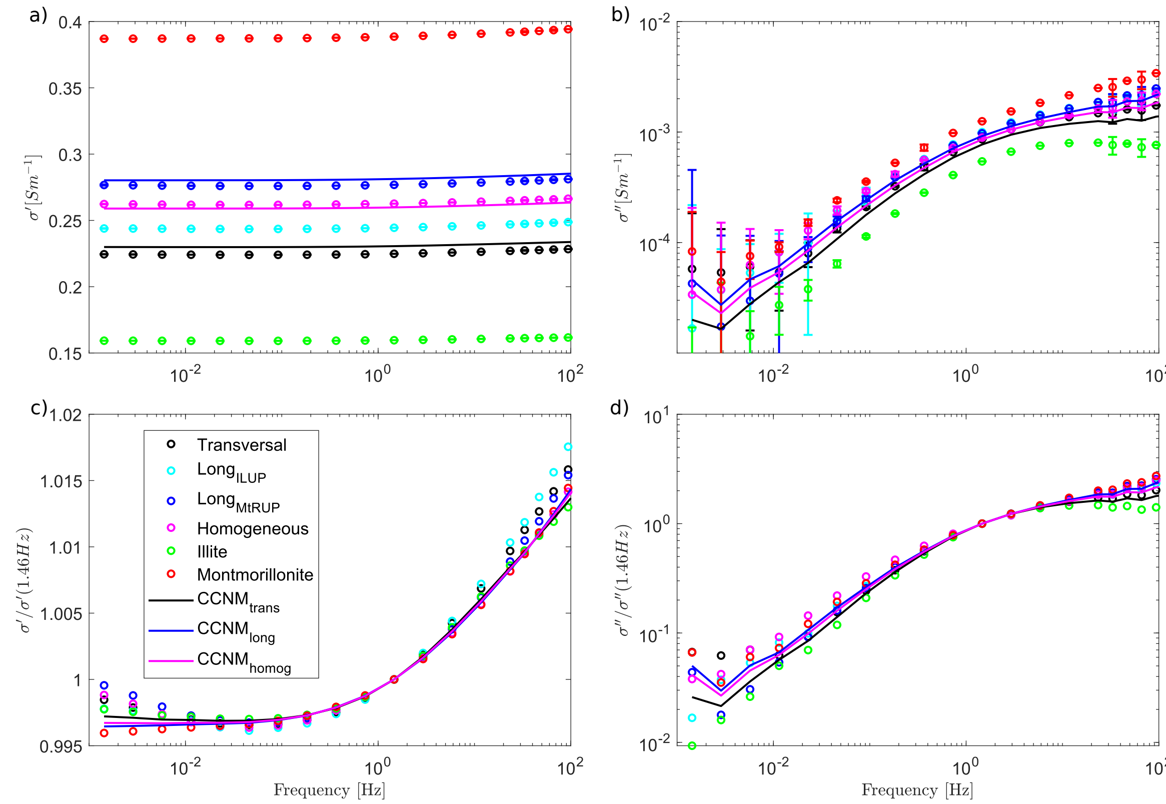


**Figure 4.** a) Real conductivity measurements and conductance network models, b) imaginary conductivity measurements overlain by the conductance network models, c) normalized real conductivity of the measurements and conductance network models, and d) normalized imaginary conductivity of the measurements and conductance network models of the illite and red montmorillonite mixtures. Long$_{\text{IL-UP}}$ and Long$_{\text{MtR-UP}}$ refer to the longitudinal mixtures (parallel), with illite and red montmorillonite near the potential electrodes, respectively. CCNM-trans, long, and homog refer to the complex conductance network models using the transversal, longitudinal and homogeneous arrangements, respectively.

0.5, but when the electrode volume has been removed, we obtain $c = 0.5005$ (see equation 2). Therefore, we used Voigt's model for an illite in the top half (IL-UP, in contact with the potential electrodes), and a model with the red montmorillonite on the top half (MtR-UP). In figure 5, we present these models with a different $c$ value as Voigt$_{IL-UP}$ and Voigt$_{MtR-UP}$, both are too close to each other and that it is impossible to discern the difference a $c$ value of 0.0005 makes in the model. In general for the mixing laws, we see that overall the modeled values are affected by both members of the mixtures, the red montmorillonite and illite (see Figs 5a and b). As to the shape of the spectra (lack of a peak near 10 Hz for the imaginary part of the conductivity), if we take a look at Figs 5c and d, we could interpret that the shape of the curve of both Voigt's models are more affected by the red montmorillonite content, and so are the data. That is, we are not able to properly model the dataset with illite in the top half (illite in contact with the potential electrodes). On the other hand, both Reuss and self-consistent models seem to be affected by both the illite and red montmorillonite content, in the shape of their spectra (closer to presenting a peak near 10 Hz). However, the corresponding datasets do not seem to follow the same trend as for the shape of the spectra. It is worth mentioning that these measurements contain errors that are inherent to the nature of experimental data.

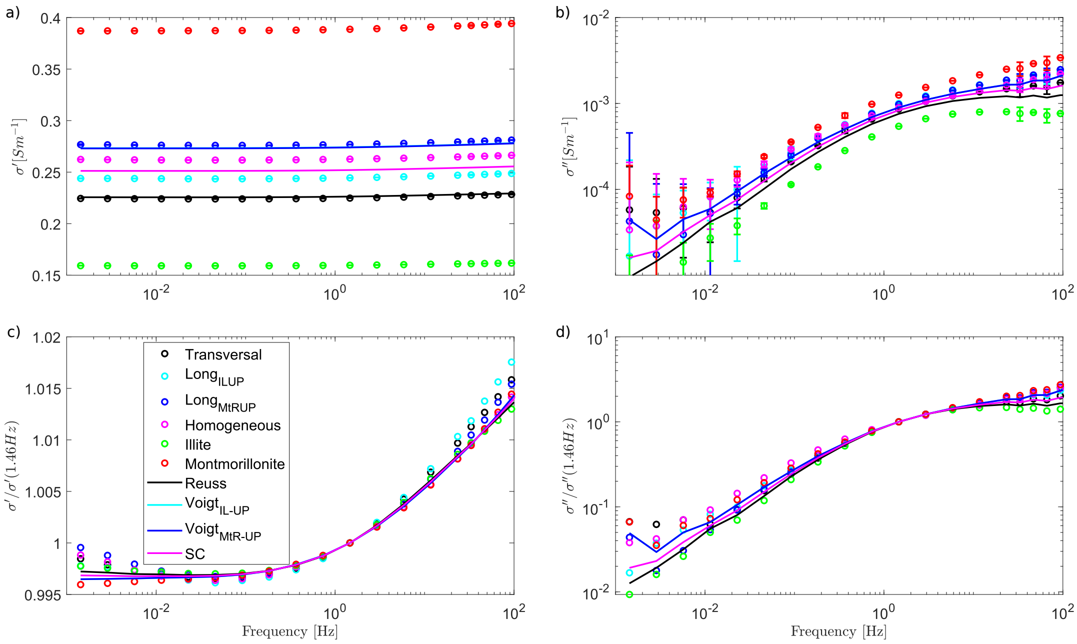


**Figure 5.** a) Real conductivity measurements, b) imaginary conductivity measurements overlain by the Reuss, Voigt (IL-UP and MtR-UP), and self-consistent models, c) normalized real conductivity of the measurements, and d) normalized imaginary conductivity of the measurements overlain by the normalized Reuss, Voigt (IL-UP and MtR-UP), and self-consistent models. $\mathrm{Long}_{\mathrm{IL\text{-}UP}}$ and $\mathrm{Long}_{\mathrm{MtR\text{-}UP}}$ refer to the longitudinal mixtures (parallel), with illite and red montmorillonite near the potential electrodes, respectively. Reuss and Voigt refer to their corresponding models, and SC corresponds to the self-consistent model. $\mathrm{Voigt}_{\mathrm{IL\text{-}UP}}$ refers to a model with illite filling the half with the potential electrodes, and $\mathrm{Voigt}_{\mathrm{MtR\text{-}UP}}$ to the red montmorillonite filling the half with the potential electrodes; these models are superposed.

## 5 Discussion

In this study we measured the SIP signature of a homogeneous and three heterogeneous mixtures of two types of clays, illite and red montmorillonite. The heterogeneous mixtures are arranged in a transversal and longitudinal manner. In addition to the SIP measurements, we tested the validity of traditional mixing laws and complex conductance network models to predict the resulting electrical signature of heterogeneous and homogeneous mixtures. We compared both modeling approaches to try to understand the benefits and pitfalls of each approach. Mixing laws constitute a classical approach for this kind of problems, at least for the real value component (see for instance Gueguen & Palciauskas, 1994). In this section, we discuss the difference between the two types of longitudinal measurements. We also interpret the polarization responses of the mixtures, as to which clay type is dominant. Additionally, we discuss the content of red montmorillonite in the mixtures above which the polarization is dominated by the red montmorillonite. Finally, we compare our data and modeling approaches to other approaches already published in the literature.

To better understand the reason of the difference between both longitudinal measurements, we created a numerical model (with finite elements) of the electric potential and the current density distribution within the samples (heterogeneous longitudinal mixture with montmorillonite on top, then illite on top, and finally the transversal mixture, see Fig. 6). For this numerical model, we used the COMSOL Multiphysics software to perform the numerical modeling. We created a domain with the dimensions of our sample holder, and within the domain and subdomains (top/bottom and side portions) we specified an electrical conductivity as to replicate the measurements (see Figs. 2 b, c, and d). Within COMSOL, we used the electrical currents interface which uses current conservation as the physical principle. We applied a boundary condition on the electric potential on the sides of the cylinders (see Fig. 6), and located the potential difference measurements in the exact same position as where the measuring electrodes are in the laboratory measurements. We did not use the complex nature of our measurements for this model, but it is an interesting idea for future work. We can see that there is a higher current density on the montmorillonite half, for the longitudinal samples (Figs 6a and b). This makes sense, as montmorillonite is more conductive (0.39 S $m^{-1}$ at 1.46 Hz) than illite (0.16 S $m^{-1}$ at 1.46 Hz). For the transversal sample (Fig. 6c), the current density seems unchanged from one half to the other. This also makes sense, as all the current lines that pass through the montmorillonite half have to pass through the illite half. The fact that there is a higher current density on the montmorillonite half for the longitudinal arrangements could explain why we see a mismatch in the longitudinal measurements (Fig. 3), for both amplitude and phase. In the first case (montmorillonite next to the measuring electrodes) there is a higher current density on the side of the measuring electrodes whereas in the second case there is less (illite next to the measuring electrodes).

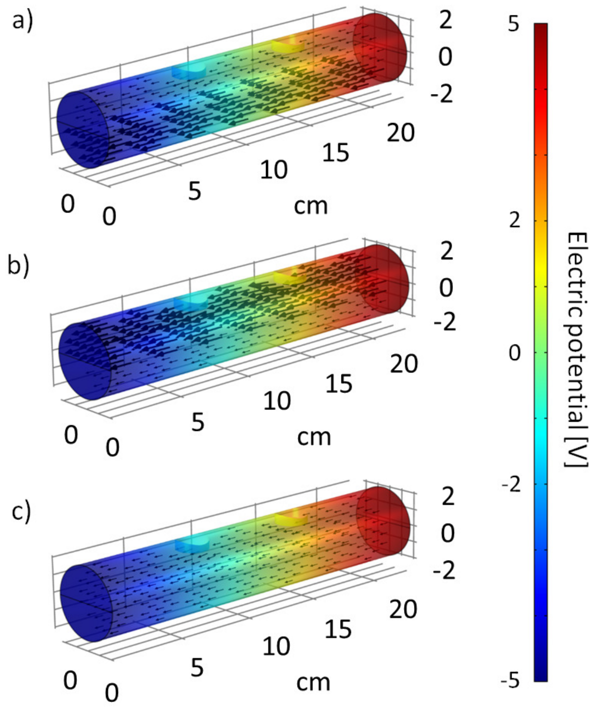


**Figure 6.** Numerical modeling of the electric potential distribution of heterogeneous clay samples for: a) longitudinal sample (parallel) with illite on the top portion, b) red montmorillonite on the top portion and c) a transversal sample (series) with equal volumetric amounts of illite and red montmorillonite. All models were subjected to an electric potential difference of -5 to 5 V. The arrows are a graphic representation of the current density and their size depends on the amplitude of the current density.

An interesting result from the SIP measurements (see Fig. 3), is that the real conductivity of the mixtures is closer to the signature of the illite than the montmorillonite (in amplitude), although the amplitude of the conductivity of the montmorillonite is larger than that of the illite (see Fig. S5 from the supplementary information). On the other hand, the shape of the spectra of the mixtures resembles more for both conductivities (real and imaginary) the shape of the montmorillonite. That is the lack of a peak near 10 Hz for the imaginary part and an increase in the real conductivity near $5 \times 10^2$ Hz. As to physical explanations of this phenomenon, we could say that perhaps the specific surface area of the montmorillonite is more important for montmorillonite than for illite (from 390 to 780 $m^2/g$ according to Tournassat et al., 2013). Thus, we can think that simply the component that polarizes the most (red montmorillonite in this case) dominates the polarization of the mixtures. However, the amplitude of the conductivity will be affected by both components of the mixture, closer to the amplitude of the conductivity of the illite, but affected by both illite and red montmorillonite nonetheless. We would have liked to compare these results to others presented in the literature, however, to the best of our knowledge, measurements as the ones presented in this study have not been reported.

We therefore propose that, for these mixture of illite and red montmorillonite, the red montmorillonite dominates the polarization. We wanted to test if a percolation threshold exists, and if so, at which percentage of montmorillonite it lies. That is that montmorillonite dominates polarization as long as a certain amount is present in the mixture. To test for this hypothesis, we performed numerical simulations of a homogeneous complex conductance network with different amounts of illite; from 100% red montmorillonite, to 10% illite, then 20%, all the way to 100% illite. The results of this test are presented in Fig. 7. It is hard to determine where the inflexion point is, from Fig. 7 we see a smooth transition. We cannot determine an inflexion point nor a threshold value. However, we can say that in homogeneous mixtures of illite and montmorillonite at varying percentages, the SIP signature varies smoothly.

We calculated the difference ($\Delta\sigma = \sqrt{(\sigma_{model} - \sigma_{data})^2}$) between the models (both conductance networks, and Voigt, Reuss, and self consistent models) and the measured SIP data (see Fig. 8). We were unable to calculate a difference for the longitudinal datasets and the conductance network models, as there is no measuring point in the complex conductance network models. However, for the Voigt models, we calculated this difference between the dataset with the illite next to the potential electrodes, and the model with the volume fraction corresponding to that of having the space for the electrodes on its half. We did this calculation in the same manner for the red montmorillonite, next to the potential electrodes. This calculation determines how good the fit is, so how the val-

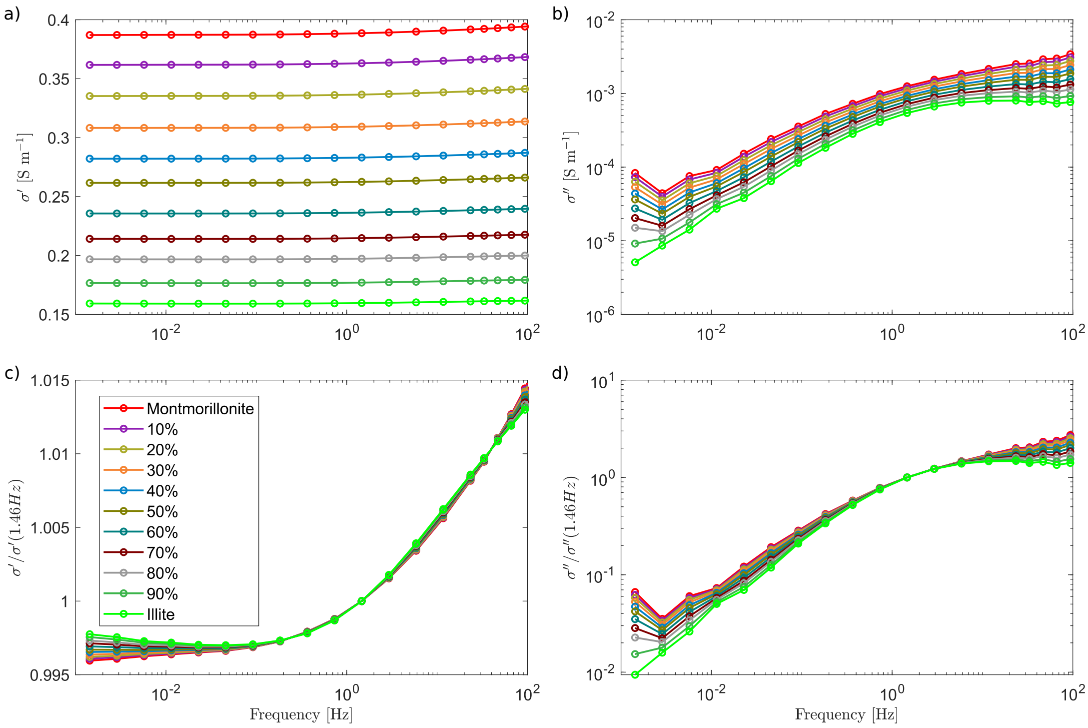


**Figure 7.** SIP modeling with complex conductance networks of a homogeneous mixture of illite and red montmorillonite, varying in illite content (from 0%, to 10%, all the way to 100%): a) real and b) imaginary part of the conductivity, c) real and d) imaginary normalized by their respective conductivities at 1.46 Hz.

ues of the models approached the measured data, it does not really portray how well the model is able to predict the presence of polarization peaks at a particular frequency. For the real part of the conductivity (Fig. 8a), definitely the Reuss, the Voigt with the red montmorillonite next to the potential electrodes and the complex conductance network of the homogeneous mix fit the data the best. For the imaginary part of the data (Fig. 8b), at frequencies above $10^1$ Hz, the best fit is overall from the conductance network approach and the Voigt model with illite next to the potential electrodes. For lower frequencies, it is hard to say for the imaginary conductivity. As for the shape of the curves, comparing Figs 4c and d, and 5c and d, it seems that the conductance network models follow better the trend of the data, that is the presence or not of a peak at a particular frequency. Overall, we can say that the use of mixing laws for the complex conductivity is valid. Here, we make use of both the real and imaginary parts of the conductivity and the predicting capabilities of these approaches with the complex conductivity, based on Figs 5 and 8, that show a good fit between data and model. Furthermore, also the use of complex conductance network models for complex conductivity seems valid, as seen in Figs 4 and 8, also the fit between data and model are quite good.

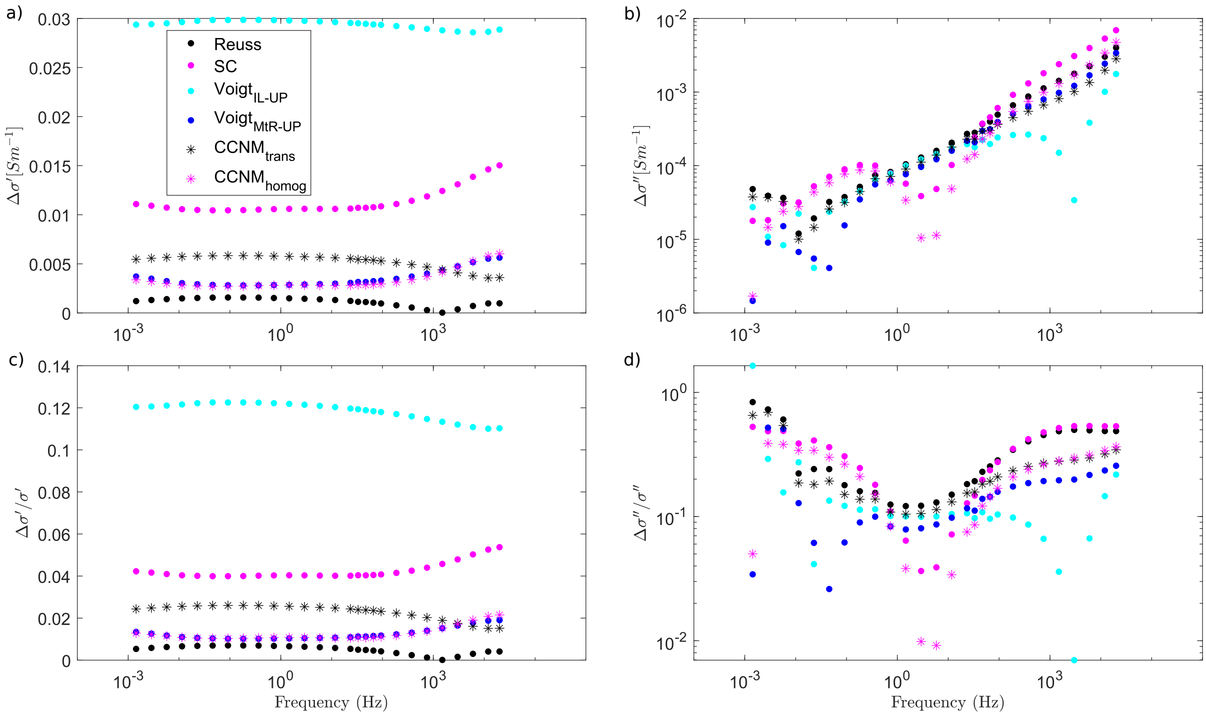


**Figure 8.** Comparison between the Reuss, Voigt, and self-consistent (SC) approach to the conductance network models, with the a) real and b) imaginary part of the electrical conductivity, c) normalized real and d) imaginary electrical conductivity.

One of the few studies that deal with modeling the electrical signature of anisotropic samples using impedance networks was done by Madden (1976). He created different conductance networks, trying to represent different anisotropic media through pore networks, he took a pore size distribution into account and obtained a conductivity distribution for different scales of anisotropy in a simulated rock sample. He concludes that a geometric mean of the components of the mixture is a good predictor of the physical parameters of a rock (electrical parameters for the purposes of this study), but this approach does not take into account the possible complexity of the inner-connectivity of the pores or cracks of the rock sample. This could greatly alter the resulting electrical conductivity of a rock sample. This is clearly in agreement with our results, as the Reuss and Voigt models with the red montmorillonite next to the potential electrodes models give a better fit to the measured real conductivity than the conductance network models (Fig. 8a).

Additionally, mixing laws represent a classical approach for this kind of problems, at least for the real value component (Gueguen & Palciauskas, 1994). We also agree that models that do not take into account the complex connectivity of a clay sample cannot fully represent the complexity of its polarization. Here, we use the definition of anisotropy used by Lynn & Michelena (2011), which state that the measured value depends on the direction of the measurement itself.

Furthermore, Winchen et al. (2009) modeled the complex conductivity signature of a 2D anisotropic system. They suggest that anisotropy affects the electrical signature of such systems and thus it should always be taken into account. Al-Hazaimay et al. (2016) used the modeling approach of Winchen et al. (2009) and paired it with SIP measurements in the laboratory of a synthetic anistropic system. They use a correction factor to be able to compare 2D models and 3D SIP measurements. Moreover, Al-Hazaimay et al. (2016) mention that electrical anisotropy should always be considered when performing geo-electrical measurements as they clearly affect the measured signature in the laboratory. This agrees with our observations. The use of both numerical and laboratory experiments prove to be useful to better understand the electrical signature of heterogeneous systems in both Al-Hazaimay et al. (2016) and our study. This proves that it is important to understand the small scale (laboratory scale) to be able to better interpret the field scale using geo-electrical measurements. There is still a need to bridge scale gaps from the pore to the laboratory scale and from the laboratory scale to the field scale, but we think that this study is a good step forward in that direction. Better understanding the resulting electrical conductivity of a mixture with a simple geometry (layering) in the laboratory will help us better understand similar structures in the field.

In this contribution we have presented a way to model the resulting electrical conductivity of a mixture of two clays, red montmorillonite and illite, and compare it to SIP measurements of heterogeneous mixtures of clays. However, an interesting next step would be the inverse problem. Determining from a given SIP spectrum the types of clays that conform the sample, knowing what the individual SIP spectra of the components look like. Although this would prove to be a complex task, because as presented in this contribution, layering and volumetric content, among other elements affect the measured SIP signature of a non-consolidated clay laboratory sample.

## 6 Conclusions

We present a complex conductivity dataset of illite and red montmorillonite mixtures with equal proportions of both clays, in a parallel, perpendicular, and homogeneous manner. Our data show that the polarization of all mixtures follows rather the shape of red montmorillonite, that is lacks a polarization peak near 10 Hz distinctive of the illite sample. We interpret this as montmorillonite dominating polarization over illite. We model these mixtures through traditional mixing laws and complex conductance networks. The mixing laws are better at predicting the amplitude of the conductivity response of the mixtures, but the complex conductance models allow to better predict the presence or lack of polarization peaks at particular frequencies. Both approaches are valid to predict the electrical signature of a mixture of two types of clays. There are differences between both model approaches, as mixing laws are simple arithmetic approaches but complex conductance network models take into account somewhat the connectivity of the sample.

More work needs to be done in order to determine the percolation threshold, that is the amount of montmorillonite needed in a mixture for it to dominate the polarization of the mixture. Furthermore, this study is an advance in the bridging of the pore and laboratory scales, as the complex conductance network models have successfully allowed us to predict the resulting laboratory electrical measurement from individual pore complex conductance properties.

## Data Availability

The data used in this study is available in the zenodo repository with the doi: 10.5281/zenodo.5270269.

**Acknowledgments**

The authors strongly thank the financial support of ANR EXCITING (grant ANR-17-CE06-0012) for this work and for the PhD thesis funding of A. Mendieta. We thank Jana Börner, Matthias Bücker and an anonymous reviewer for their insightful comments that helped improve the paper.

## References


Al-Hazaimay, S., Huisman, J. A., Zimmermann, E., & Vereecken, H. (2016). Using electrical anisotropy for structural characterization of sediments: an experimental validation study. *Near Surface Geophysics*, *14*(4), 357–369. doi: 10.3997/1873-0604.2016026

Bairlein, K., Bücker, M., Hördt, A., & Hinze, B. (2016). Temperature dependence of spectral induced polarization data: experimental results and membrane polarization theory. *Geophysical Journal International*, *205*(1), 440–453. doi: 10.1093/gji/ggw027

Bernabe, Y. (1995). The transport properties of networks of cracks and pores. *Journal of Geophysical Research*, *100*(B3), 4231–4241. doi: 10.1029/94JB02986

Berryman, J. G. (1995). Mixture theories for rock properties. In T. J. Ahrens (Ed.), *Rock physics & phase relations: a handbook of physical constants* (pp. 205–228). Washington, D.C.: American geophysical union. doi: /10.1029/RF003p0205

Breede, K., Kemna, A., Esser, O., Zimmermann, E., Vereecken, H., & Huisman, J. A. (2012). Spectral induced polarization measurements on variably saturated sand-clay mixtures. *Near Surface Geophysics*, *10*(6), 479–489. doi: 10.3997/1873-0604.2012048

Bücker, M., Flores Orozco, A., Undorf, S., & Kemna, A. (2019). On the role of Stern- and diffuse-layer polarization mechanisms in porous media. *Journal of Geophysical Research: Solid Earth*, *124*(6), 5656–5677. doi: 10.1029/2019JB017679

Bücker, M., & Hördt, A. (2013a). Analytical modelling of membrane polarization with explicit parametrization of pore radii and the electrical double layer. *Geophysical Journal International*, *194*(2), 804–813. doi: 10.1093/gji/ggt136

Bücker, M., & Hördt, A. (2013b). Long and short narrow pore models for membrane polarization. *Geophysics*, *78*, E299–E314. doi: 10.1190/GEO2012-0548.1

Cosenza, P., Ghorbani, A., Revil, A., Zamora, M., Schmutz, M., Jougnot, D., & Florsch, N. (2008). A physical model of the low-frequency electrical polarization of clay rocks. *Journal of Geophysical Research: Solid Earth*, *113*(B8), 1–9. doi: 10.1029/2007JB005539

Day-Lewis, F. D., Linde, N., Haggerty, R., Singha, K., & Briggs, M. A. (2017). Pore network modeling of the electrical signature of solute transport in dual-domain media. *Geophysical Research Letters*, *44*(10), 4908–4916. doi:

10.1002/2017GL073326

de Lima, O. A., & Sharma, M. M. (1992). A generalized Maxwell-Wagner theory for membrane polarization in shaly sands. *Geophysics*, *57*(3), 431–440. doi: 10.1190/1.1443257

Ghorbani, A., Cosenza, P., Revil, A., Zamora, M., Schmutz, M., Florsch, N., & Jougnot, D. (2009). Non-invasive monitoring of water content and textural changes in clay-rocks using spectral induced polarization: A laboratory investigation. *Applied Clay Science*, *43*(3), 493–502. doi: 10.1016/j.clay.2008.12.007

Gueguen, Y., & Palciauskas, V. (1994). *Introduction to the Physics of Rocks*. Princeton University Press.

Hashin, Z. (1968). Assessment of the self consistent scheme approximation: conductivity of particulate composites. *Journal of Composite Materials*, *2*(3), 284–300. doi: 10.1177/002199836800200302

Hayley, K., Bentley, L. R., Gharibi, M., & Nightingale, M. (2007). Low temperature dependence of electrical resistivity: Implications for near surface geophysical monitoring. *Geophysical Research Letters*, *34*(18), 1–5. doi: 10.1029/2007GL031124

Iravani, M. A., Deparis, J., Davarzani, H., Colombano, S., Guérin, R., & Maineult, A. (2020). The influence of temperature on the dielectric permittivity and complex electrical resistivity of porous media saturated with DNAPLs: A laboratory study. *Journal of Applied Geophysics*, *172*, 1–11. doi: 10.1016/j.jappgeo.2019.103921

Jougnot, D. (2020). *Developing hydrogeophysics for critical zone studies, importance of heterogeneities and processes at the mesoscopic scale* (Habilitation dissertation, Sorbonne Université, Paris, France). doi: 10.5281/zenodo.5517748

Jougnot, D., Ghorbani, A., Revil, A., Leroy, P., & Cosenza, P. (2010). Spectral induced polarization of partially saturated clay-rocks: a mechanistic approach. *Geophysical Journal International*, *180*(1), 210–224. doi: 10.1111/j.1365-246X.2009.04426.x

Jougnot, D., Jiménez-Martínez, J., Legendre, R., Le Borgne, T., Méheust, Y., & Linde, N. (2018). Impact of small-scale saline tracer heterogeneity on electrical resistivity monitoring in fully and partially saturated porous media: Insights from geoelectrical milli-fluidic experiments. *Advances in Water Resources*, *113*, 295–309. doi: 10.1016/j.advwatres.2018.01.014

Jougnot, D., Mendieta, A., Leroy, P., & Maineult, A. (2019). Exploring the effect of the pore size distribution on the streaming potential generation in saturated porous media, insight from pore network simulations. *Journal of Geophysical Research: Solid Earth*, *124*(6), 5315–5335. doi: 10.1029/2018JB017240

Kemna, A., Binley, A., Cassiani, G., Niederleithinger, E., Revil, A., Slater, L., ... Zimmermann, E. (2012). An overview of the spectral induced polarization method for near-surface applications. *Near Surface Geophysics*, *10*(6), 453–468. doi: 10.3997/1873-0604.2012027

Kenkel, J., Hördt, A., & Kemna, A. (2012). 2D modelling of induced polarization data with anisotropic complex conductivities. *Near Surface Geophysics*, *10*(6), 533–544. doi: 10.3997/1873-0604.2012050

Kirchhoff, G. (1845). Ueber den Durchgang eines elektrischen Stromes durch eine Ebene, insbesondere durch eine kreisförmige. *Annalen der physik und chemie*, *140*, 497–514. doi: 10.1002/andp.18451400402

Knight, R. J., & Endres, A. L. (2005). An introduction to rock physics principles for near-surface geophysics. In D. K. Butler (Ed.), *Near-surface geophysics* (pp. 31–65). Tuls, Oklahoma: Society of Exploration Geophysicists. doi: 10.1190/1.9781560801719.ch3

Kremer, T., Schmutz, M., Maineult, A., & Agrinier, P. (2016). Laboratory monitoring of CO2 injection in saturated silica and carbonate sands using spectral induced polarization. *Geophysical Journal International*, *207*(2), 1258–1272. doi: 10.1093/gji/ggw333

Leroy, P., Weigand, M., Mériguet, G., Zimmermann, E., Tournassat, C., Fagerlund, F., ... Huisman, J. A. (2017). Spectral induced polarization of Na-montmorillonite dispersions. *Journal of Colloid And Interface Science*, *505*, 1093–1110. doi: 10.1016/j.jcis.2017.06.071

Loewer, M., Günther, T., Igel, J., Kruschwitz, S., Martin, T., & Wagner, N. (2017). Ultra-broad-band electrical spectroscopy of soils and sediments-a combined permittivity and conductivity model. *Geophysical Journal International*, *210*(3), 1360–1373. doi: 10.1093/gji/ggx242

Lynn, H., & Michelena, R. J. (2011). Introduction to this special section: Practical applications of anisotropy. *The Leading Edge*, *30*(7), 726–730. doi: 10.1190/1.3609086

Madden, T. R. (1976). Random networks and mixing laws. *Geophysics*, *41*(6 A), 1104–1125. doi: 10.1190/1.2035907

Maineult, A. (2018a). Corrigendum to "Upscaling of spectral induced polarization response using random tube networks", by Maineult et al. (2017, Geophysical Journal International, 209, pp. 948–960). *Geophysical Journal International*, *213*, 1296–1296. doi: 10.1093/gji/ggy052

Maineult, A., Gurin, G., & Titov, K. (2021). Impedance network modelling to simulate the chargeability of sand-pyrite mixtures. In *27th european meeting of environmental and engineering geophysics* (pp. 1–5). Bordeaux, France: European Association of Geoscientists and Engineers. doi: 10.3997/2214-4609.202120050

Maineult, A., Jougnot, D., & Revil, A. (2018b). Variations of petrophysical properties and spectral induced polarization in response to drainage and imbibition: A study on a correlated random tube network. *Geophysical Journal International*, *212*, 1398–1411. doi: 10.1093/gji/ggx474

Maineult, A., Revil, A., Camerlynck, C., Florsch, N., & Titov, K. (2017). Upscaling of spectral induced polarization response using random tube networks. *Geophysical Journal International*, *209*, 948–960. doi: 10.1093/gji/ggx066

Mendieta, A., Jougnot, D., Leroy, P., & Maineult, A. (2021). Spectral induced polarization characterization of non-consolidated clays for varying salinities - an experimental study. *Journal of Geophysical Research: Solid Earth*, *126*(4). doi: 10.1029/2020jb021125

Okay, G., Leroy, P., Ghorbani, A., Cosenza, P., Camerlynck, C., Cabrera, J., ... Revil, A. (2014). Spectral induced polarization of clay-sand mixtures : Experiments and modeling. *Geophysics*, *79*(6), 353–375. doi: 10.1190/geo2013-0347.1

Pelton, W., Ward, S. H., Hallof, P. G., Sill, W. R., & Nelson, P. H. (1978). Mineral discrimination and removal of inductive coupling with multifrequency IP. *Geophyics*, *43*(3), 588–609. doi: 10.1190/1.1440839

Pride, S. (1994). Governing equations for the coupled electromagnetics and acoustics of porous media. *Physical Review B*, *50*(21), 15678–15696.

Renard, P., & de Marsily, G. (1997). Calculating equivalent permeability: a review. *Advances in Water Resources*, *20*(5-6), 253–278. doi: 10.1016/S0309-1708(96)00050-4.

Reuss, A. (1929). Berechnung der Fließgrenze von Mischkristallen auf Grund der

Plastizitätsbedingung für Einkristalle. *Zeitschrift für Angewandte Mathematik und Mechanik*, *9*(1), 49–58. doi: 10.1002/zamm.19290090104

Revil, A. (2012). Spectral induced polarization of shaly sands: Influence of the electrical double layer. *Water Resources Research*, *48*(2), 1–23. doi: 10.1029/2011WR011260

Revil, A., Linde, N., Cerepi, A., Jougnot, D., Matthäi, S., & Finsterle, S. (2007). Electrokinetic coupling in unsaturated porous media. *Journal of Colloid and Interface Science*, *313*(1), 315–327. doi: 10.1016/j.jcis.2007.03.037

Revil, A., Woodruf, W. F., Torres-Verdín, C., & Prasad, M. (2013). Complex conductivity tensor of anisotropic hydrocarbon-bearing shales and mudrocks. *Geophysics*, *78*(6), E299–E314. doi: 10.1190/GEO2012-0548.1

Stebner, H., Halisch, M., & Hördt, A. (2017). Simulation of membrane polarization of porous media with impedance networks. *Near Surface Geophysics*, *15*(6), 563–578. doi: 10.3997/1873-0604.2017054

Tournassat, C., Grangeon, S., Leroy, P., & Giffaut, E. (2013). Modeling specific pH dependent sorption of divalent metals on montmorillonite surfaces. A review of pitfalls, recent achievements and current challenges. *American Journal of Science*, *313*(5), 395–451. doi: /10.2475/05.2013.01

Voigt, W. (1910). *Lehrbuch der Kristallphysik*. Leipzig, Germany: Teubner-Verlag.

Wenk, H. R., Voltolini, M., Mazurek, M., Van Loon, L. R., & Vinsot, A. (2008). Preferred orientations and anisotropy in shales: Callovo-oxfordian shale (France) and opalinus clay (Switzerland). *Clays and Clay Minerals*, *56*(3), 285–306. doi: 10.1346/CCMN.2008.0560301

Winchen, T., Kemna, A., Vereecken, H., & Huisman, J. A. (2009). Characterization of bimodal facies distributions using effective anisotropic complex resistivity : A 2D numerical study based on Cole-Cole models. *Geophysics*, *74*(3), A19–A22. doi: 10.1190/1.3113986

Woodruff, W. F., Revil, A., & Torres-Verdín, C. (2014). Laboratory determination of the complex conductivity tensor of unconventional anisotropic shales. *Geophysics*, *79*(5), E183–E200. doi: 10.1190/geo2013-0367.1

Zanetti, C., Weller, A., Vennetier, M., & Mériaux, P. (2011). Detection of buried tree root samples by using geoelectrical measurements: A laboratory experiment. *Plant Soil*, *339*(1), 273–283. doi: 10.1007/s11104-010-0574-0

Zimmermann, E., Kemna, A., Berwix, J., Glaas, W., Münch, H. M., & Huisman, J. A. (2008). A high-accuracy impedance spectrometer for measuring sediments with low polarizability. *Measurement Science and Technology*, *19*(10), 1–9. doi: 10.1088/0957-0233/19/10/105603

Zisser, N., Kemna, A., & Nover, G. (2010). Dependence of spectral-induced polarization response of sandstone on temperature and its relevance to permeability estimation. *Journal of Geophysical Research: Solid Earth*, *115*(9), 1–15. doi: 10.1029/2010JB007526